Available online at www.sciencedirect.com
ScienceDirect
Journal of Solid State Chemistry 179 (2006) 3033–3044
JOURNAL OF SOLID STATE CHEMISTRY
www.elsevier.com/locate/jssc

Visible light-sensitive yellow $TiO_{2-x}N_x$ and Fe–N co-doped $Ti_{1-y}Fe_yO_{2-x}N_x$ anatase photocatalysts

K.S. Rane[a,*], R. Mhalsiker[a], S. Yin[b], T. Sato[b], Kuk Cho[c], E. Dunbar[c], Pratim Biswas[c]

[a]*Department of Chemistry, Goa University, Panaji City, Goa 403206, India*
[b]*Institute of Multidisciplinary Research for Advanced Materials, Tohoku University, 2-1-1 Katachira, Aoba-ku, Sendai, Miyagi 980-8577, Japan*
[c]*Environmental Engineering Science, School of Engineering and Applied Sciences, Washington University in St. Louis, One Brooking Drive, Campus Box 1180, St. Louis, MO 63130-4899, USA*

Received 10 March 2006; received in revised form 26 May 2006; accepted 28 May 2006
Available online 3 June 2006

Abstract

Nitrogen substituted yellow colored anatase $TiO_{2-x}N_x$ and Fe–N co-doped $Ti_{1-y}Fe_yO_{2-x}N_x$ have been easily synthesized by novel hydrazine method. White anatase $TiO_{2-\delta}$ and N/Fe–N-doped samples are semiconducting and the presence of ESR signals at g ~1.994–2.0025 supports the oxygen vacancy and g~4.3 indicates Fe^{3+} in the lattice. $TiO_{2-x}N_x$ has higher conductivity than TiO_{2-x} and Fe/Fe–N-doped anatase and the UV absorption edge of white TiO_{2-x} extends in the visible region in N, Fe and Fe–N co-doped TiO_2, which show, respectively, two band gaps at ~3.25/2.63, ~3.31/2.44 and 2.8/2.44 eV. An activation energy of ~1.8 eV is observed in Arrhenius log resistivity vs. $1/T$ plots for all samples. All TiO_2 and Fe-doped TiO_2 show low 2-propanol photodegradation activity but have significant NO photodestruction capability, both in UV and visible regions, while standard Degussa P-25 is incapable in destroying NO in the visible region The mid-gap levels that these N and Fe–N-doped TiO_2 consist may cause this discrepancy in their photocatalytic activities.

Keywords: Hydrazine; Oxalate precursor; Oxalate-hydrazinate precursor; Anatase; Arrhenius plots; Electrical conductivity; N–TiO_2; XPS-N 1*s* peak; Photodegradation; ESR; Fe–N co-doped TiO_2

1. Introduction

Preparation strategies of spinel oxides such as MFe_2O_4 (M = Ni/Mn/Zn/Mg), perovskites, La (Sr) MO_3(M = Al/Co/Mn) and anatase TiO_2 and their effect on the magnetic, electric, catalytic and sensing properties are our main focus in the field of solid-state chemistry. Metal oxides are synthesized, in general, by the thermal decomposition of precursors such as metal hydroxides, carboxylates and their hydrazinates [1–11]. In one such preparation it was observed [10] that a white pigment-grade anatase TiO_2 synthesized from the thermal decomposition of titanium hydroxide and oxalate produced yellow colored anatase when the precursors were modified by hydrazination. Both the white and yellow TiO_2 are semiconducting [12] indicating defects in the lattice. The yellow TiO_2 showed the ultraviolet (UV) absorption edge extending into the visible (Vis.) region in diffuse reflectance spectra (DRS), while the white pigment is transparent in the region. A survey of literature [13–18] revealed a large number of papers dealing with photocatalytic activity of yellow colored TiO_2 in the Vis. region in mineralizing water and air-borne organic pollutants. The yellow color and the Vis. light absorption are attributed to the change in the band structure due to N doping. The N doping either decreases the band gap by mixing of nitrogen 2*p* states with oxygen O 2*p* states on the top of the valence band or creates N-induced mid-gap level. Hence a defective $TiO_{2-x}N_x$ may be formed when N-containing metal organic precursors are thermally heated. In our case, the titanium hydroxide and oxalate on thermal decomposition give oxygen-deficient semiconducting $TiO_{2-\delta}$, the precursors on modification with hydrazine, N_2H_4, yield the N-doped $TiO_{2-x}N_x$ or

*Corresponding author. Fax: +91 832 245 1184.
E-mail address: ksrane@unigoa.ac.in (K.S. Rane).

0022-4596/$ - see front matter © 2006 Elsevier Inc. All rights reserved.
doi:10.1016/j.jssc.2006.05.033

both oxygen-deficient and N-doped TiO_2 semiconductors [12]. It seems nitrogen is easily introduced in the lattice of anatase by the hydrazine method of synthesis. Hydrazine method of synthesis had been adopted in our earlier studies in the preparation of γ-Fe_2O_3 [3,5], $NiZnFe_2O_4$ [2], $MgFe_2O_4$ [7], $MnZnFe_2O_4$ [8] and perovskites such as $LaAlO_3$, La (Sr)AlO_3, La (Sr)MnO_3 [9]. Metal and mixed metal hydroxides and carboxylates modified with the hydrazination found to decompose at lower temperatures than those without such modifications. The titanium hydroxide and oxalate on hydrazination were also expected to decompose at lower temperatures as compared to unhydrazinated ones. The observed color change of the TiO_2 and introduction of nitrogen in the lattice of the oxide is interesting. This aspect of the introduction of nitrogen in the lattice of the TiO_2 is of interest, as spinel and perovskite oxides synthesized in our laboratories by the hydrazine method may also have in their lattice nitrogen which may have some effect on their electric and magnetic properties. In this paper, the synthesis of nitrogen-doped titanium dioxide (white and yellow) is explored to determine its photocatlytic properties. Degradation of aqueous 2-propanol and NO_x is determined, and compared to that of Degussa P-25. As both forms of the oxide (white and N doped yellow) are semiconducting and metal ions doping [19–21] modify the electronic and photocatlaytic properties of TiO_2, effect of Fe doping by oxalate method and Fe–N co-doping by hydrazine method is investigated to see whether this improves photocatalytic activity. Electron spin resonance (ESR) was used to understand the defect nature in TiO_2.

2. Experimental

2.1. Synthesis

2.1.1. Preparation of titanium hydroxide, oxalate and their hydrazinates

The synthesis of titanium hydroxide, oxalate and their hydrazine modifications was carried out using methods standardized in our previous studies [10,11]. Titanium isopropoxide in iso-propanol was added slowly into water, and the titanium hydroxide precipitate that formed was oven- and freeze-dried. For preparing titanium oxalate, commercial TiO_2 was fused with KOH in a Ni crucible and treated with concentrated HCl to precipitate out KCl. NH_3 was added to the filtrate to get titanium hydroxide, which was then separately treated with oxalic acid and ammonium oxalate. The hydrazinated titanium oxalate was prepared by adding the titanium hydroxide slurry to the well-stirred oxalic acid/hydrazine hydrate mixture in an inert atmosphere. Hydrazinated titanium hydroxide was synthesized by introducing titanium isopropoxide in isopropanol into a mixture of water and hydrazine under inert atmosphere. In another hydrazination process, the titanium hydroxide and titanium oxalate were spread over a Petri dish and kept over hydrazine hydrate, N_2H_5OH (99%), in a desiccator and the completion of the hydrazine uptake was monitored titrimetrically using KIO_3 as the titrant [22].

2.1.2. Preparation of iron containing titanium oxalates and their hydrazinates

In order to get 0.01, 0.05 and 0.1 at% of Fe-doped TiO_2, the titanium hydroxide that had been synthesized from commercial TiO_2, as described in Section 2.1.1, was dissolved in dilute HCl. A freshly prepared ferrous chloride in the requisite amount was then added and the mixture was then treated with ammonia to obtain iron-containing hydroxide. The precipitate was then separately treated with oxalic acid in air, and the mixture of oxalic acid and hydrazine hydrate in N_2 atmosphere to obtain the oxalate and hydrazinated oxalate precipitates, respectively. In another hydrazination process, the titanium oxalate containing Fe was spread over a Petri dish and kept over N_2H_5OH (99%) in a desiccator, and the completion of the hydrazine uptake was monitored titrimetrically using KIO_3 as a titrant [22].

2.2. Characterization

All samples were chemically analyzed for the quantitative presence of Ti^{4+}, $C_2O_4^{2-}$ and N_2H_4 by standard methods [22]. From the isothermal weight loss and infrared analysis (Shimadzu IR Prestige-21), chemical formulas were determined [10–12]. Using thermal analyzer (NETZSCH DSC-DTA-TG STA 409PC), the thermal paths were identified to get an idea of total decomposition of the precursors. The decomposed products were identified from X-ray diffraction (XRD) studies on ITAL APD 2000 using CuK_α radiation ($\lambda = 1.5418$ Å) and Ni filter. BET surface area measurements were made using SORPTOMETRIC model 1990 instrument and a home-built apparatus (3-point measurements). Scanning electron micrographs (SEM) were obtained on Hitachi S-4500. Transmission electron micrographs (TEM) were recorded with JEOL-JEM 100SX microscope, working at 100 kV accelerating voltage. Electron spin resonance (ESR) spectra were recorded on Varian E-line Century Series E-112 X-band ESR spectrometer using 100 kHz field modulator. tetracyanoethylene (TCNE) was used as a standard for "g" factor measurements. For electrical conductivity measurements, the oxide samples in the form of tablets of 8 mm diameter and 5 mm thickness were prepared by compressing with a hydraulic press at 10 ton of pressure. Both the sides of the pellet were pasted with silver paste and pressed between platinum electrodes and introduced into a home-built two-probe conductivity cell. The temperature variation of resistance was measured from room temperature to 600 °C using a Keithley Electrometer. Diffuse reflectance spectra (DRS) were recorded on Shimadzu UV 2450 UV–Visible Spectrometer in the wavelength range of 200–700 nm. The amount of nitrogen in the samples was determined using the oxygen–nitrogen analyzer [14] (HIROBA, EMGA, 2800). ESCA analysis was done at 298 K using MgK_α radiation with a V.G. Scientific ESCASCOPE

photoelectron spectrometer. X-ray photoelectron spectroscopy measurements were carried out over a Kratas Axis Spectrometer at a vacuum of 3×10^{-9} Torr with non-monochromatic MgK_α radiation.

2.3. Photodegradation of aqueous 2-propanol and gaseous NO_x

For studying the oxidative degradation of 2-propanol, about 50 mg of the oxide sample was suspended in an aqueous solution in a quartz cell. Prior to UV irradiation, the suspension was stirred for 30 min in an oxygen atmosphere in the dark conditions. The sample was then irradiated at 295 K using UV light ($\lambda>250$ nm) from a 100 W high-pressure Hg lamp with continuous stirring in an oxygen atmosphere. At given interval of time, the aliquots were analyzed after filtering through Millipore to remove TiO_2 particles. The products were analyzed using gas chromatography.

Photodestruction of NO_x studies were carried out as described in Ref. [14] at >290, >410 and >510 nm. About 0.12 g of the oxide sample was placed in a quartz reactor cell of internal volume 373 cm^3 and a 450 W high-pressure mercury lamp was used as the light source. The light wavelength was controlled by selecting various filters, i.e. Pyrex glass for cutting off the light of $\lambda<290$ nm, Kenko L41 Super Pro (W) filter for $\lambda<400$ nm and Fuji tri-acetyl cellulose filter for $\lambda<510$ nm. The light intensity at $\lambda<290$, 400 and 510 nm on the surface of the photocatalyst was identified as, 352, 337 and 243 $\mu mol\,m^{-2}\,s$, respectively. For photocatalytic studies, a gas mixture of $NO+Air+N_2$ (for balancing the reaction mixture) was introduced into a constant flow reactor. The activity was determined by measuring the concentration of NO gas at the outlet of the reactor. For comparison, a photocatalytic reaction was also carried out using commercially available TiO_2 (Degussa P-25).

2.4. Thermal products of the hydroxide, oxalate and their hydrazinates: codes

Based on the thermal analysis and X-ray characterization [10–12,23] all the precursors mentioned in Section 2.1 were isothermally decomposed around 400 °C for 4 h and the oxide products were coded as follows: titanium oxalate (oxal); titanium oxalate hydrazinate (oxalhyd); titanium hydroxide, both oven and freeze dried (TipOD and TipFD) and their hydrazinates (TipODH and TipFDH); 0.01, 0.05 and 0.1 at% Fe-doped titanium oxalates and their hydrazinates: 0.01 Fe-anatase/oxal, 0.05 Fe-anatase/oxal, 0.1 Fe-anatase/oxal, Hyd_0.01Fe, Hyd_0.05Fe and Hyd_0.1Fe.

3. Results and discussions

3.1. Anatase phase: Fe-doped TiO_2

The titanium hydroxide, $Ti(OH)_4\cdot1.5H_2O$ and its hydrazinate, $Ti(OH)_4\cdot N_2H_4$ and titanium oxalate, $(NH_4)_2TiO(C_2O_4)_2\cdot2H_2O$ and its hydrazinate, $(N_2H_5)_2TiO(C_2O_4)_2$ decompose completely at ~400 °C [10–12,23]. The iron-doped sample precursors also decompose at the same temperature. In general, the hydrazine-modified samples decompose earlier than that of the unmodified ones, which may be due to explosive decomposition. The oxide products of the oxalate (oxal) and both oven-dried and freeze-dried hydroxides (TipOD/TipFD) are white, while the thermal product of titanium oxalate hydrazinate (oxalhyd) is yellow color. The d_{hkl} values that obtained by XRD (Fig. 1) match well with the ICDD Card [24] of anatase TiO_2. The thermal products of iron-doped oxalate and hydrazinate: 0.01Fe-anatase/oxal; 0.05Fe-anatase/oxal; 0.1Fe-anatase/oxal, Hyd_0.01Fe; Hyd_0.05Fe; Hyd_0.1Fe are brown in color and show anatase type phase (Fig. 1).

3.2. BET surface area, nitrogen content, ESCA and DRS: band gap

The BET surface areas of all the TiO_2 samples are found to be in the range of 42–107 $m^2\,g^{-1}$. The white anatase obtained from the thermal decomposition of $(NH_4)_2TiO(C_2O_4)_2.2H_2O$ showed a surface area of 65.9 $m^2\,g^{-1}$, while the yellow oxide product of hydrazinated complex, $(N_2H_5)_2TiO(C_2O_4)_2$ indicated an enhanced value of 107.6 $m^2\,g^{-1}$. Low temperature-explosive decomposition of the hydrazine complexes, in general, found in our studies [1–11] lead to products with small particle size and large surface areas. A representative TEM of yellow TiO_2 and Fe–N co-doped, Hyd_0.01Fe, obtained by hydrazine method in Fig. 2 confirm a fine nature of particles in the nanometer-sized range, while the white anatase from titanium oxalate has agglomerated particles. SEM studies too reveal the presence of an agglomerated particles in the case of products of oxalate precursors.

3.2.1. Nitrogen: O_2–N_2 analysis and XPS

The hydrazine that is released by low temperature decomposition of $(N_2H_5)_2TiO(C_2O_4)_2$ reacts with the atmospheric oxygen and liberates enormous [25]

$$N_2H_4+O_2\rightarrow N_2+H_2O,\quad \Delta H=-621\,kJ\,mol^{-1}. \qquad (1)$$

This energy is sufficient to exothermically decompose the complex devoid of hydrazine at much lower temperature than $(NH_4)_2TiO(C_2O_4)_2\cdot2H_2O$, and the resultant particles thus formed are of fine nature. The nitrogen contents measured on all anatase and Fe-doped samples prepared by the hydrazine method showed the values in the range of 0.425–0.95%, and the highest value is observed for the yellow anatase obtained from titanium oxalate hydrazinate (oxalhyd), while the oxide products of the oxalate samples did not show any presence of nitrogen (Table 1). However, the 0.95% nitrogen content of yellow anatase reduced to 0.30% on calcining at 400 °C, the titanium oxalate hydrazinate in nitrogen atmosphere (oxalhyd 400 °C/N_2) and the similar but marginal decrease from 0.13% to 0.1% is

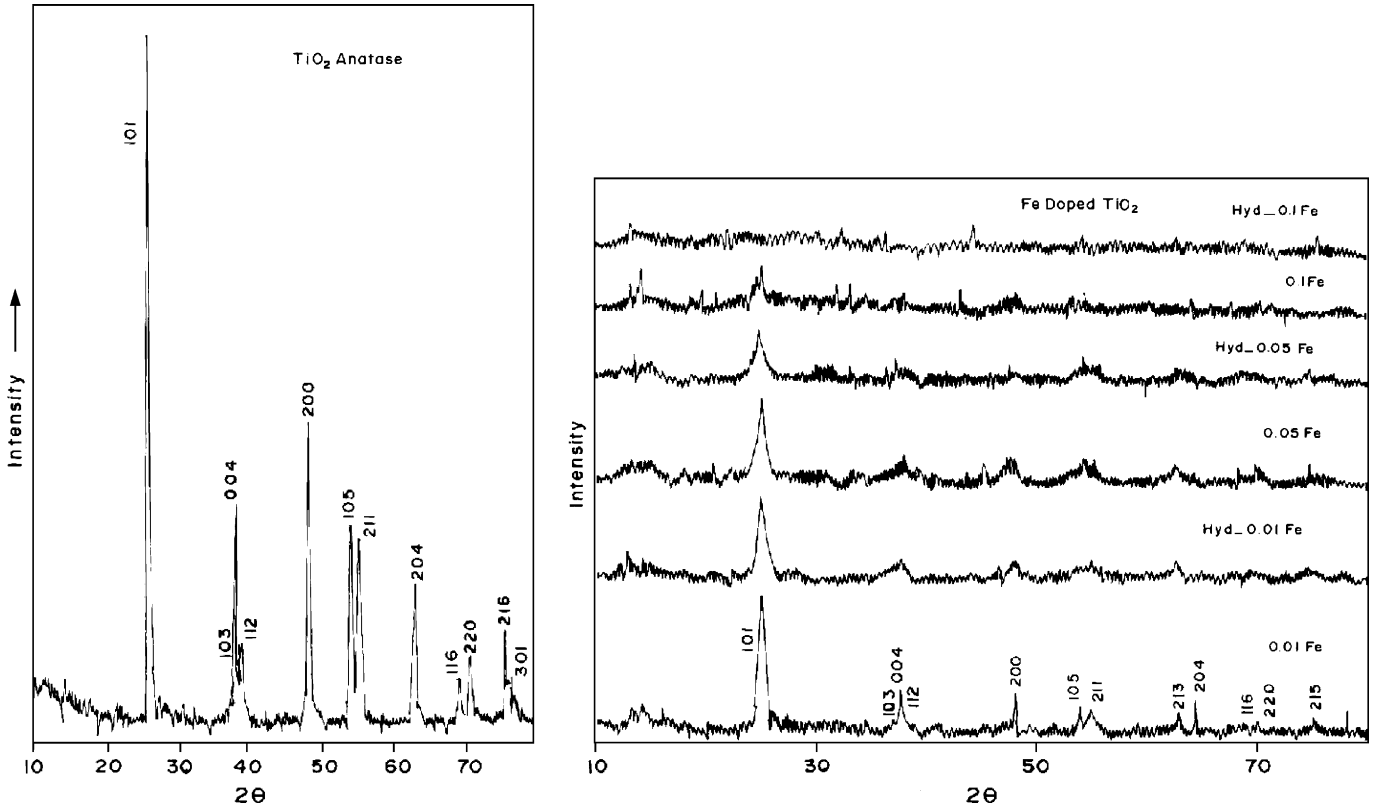

Fig. 1. X-ray diffraction pattern of anatase and Fe-doped anatase.

observed for yellow TipODH. The hydrazine method of preparation introduces nitrogen in the lattice easily, as during decomposition of N_2H_4 that released reacts with atmospheric O_2 and produces the N_2 and H_2O (Eq. (1)). The nitrogen thus formed in situ easily gets trapped in the lattice of the oxide. Thus, the yellow anatase has the formula, $TiO2_{-x}N_x$ and Fe–N-doped anatase may have the composition, $Ti_{1-y}Fe_yO_{2-x}N_x$. Although the nitrogen content measured by oxygen–nitrogen analyzer indicates its presence in the yellow colored TiO_2 and Fe–N co-doped TiO_2, the ESCA study carried out on ESCASCOPE did not give clear indication of the presence of N 1*s* peak [18,21,26,27] at 396 eV. However, a peak centered ~400.54 eV is observed in Kratas Axis Spectrometer, Fig. 3a for the yellow N-doped TiO_2 (oxalhyd) and ~400.27 eV, Fig. 3a for Fe–N co-doped TiO_2 (Hyd_0.1Fe) which contain, respectively, 0.95% and 0.796% nitrogen (Table 1).

Sakthivel and Kisch [13,28] observed no anionic-like nitrogen species around 396 eV, rather a N 1*s* peak at 404 eV attributed to hyponitrite type nitrogen. Valentin et al [29] observed N 1*s* core level at 400 eV and attributed it to a lower valence state of nitrogen. Gole et al. [16] and Chen and Burda [30] observed the N 1*s* level at 401-3 eV and considered it to be N–Ti–O linkage in the lattice. Thus, the presence of nitrogen in the lattice can be ascertained. Further, Satish et al. [31] from their observations of Ti $2p_{3/2}$ level at 459.3 for TiO_2 and that for N–TiO_2 at 458.5 eV attributed the lower binding energy (BE) for N–TiO_2 to different electronic interaction of Ti with nitrogen anion compared to the oxygen anion. They suggested a considerable modification of the lattice due to N substitution. In our studies, we find the Ti $2p_{3/2}$ level at ~458.187 eV (Fig. 3c) for N-doped yellow TiO_2 (oxalhyd) and ~458.194 eV (Fig. 3c for Fe–N co-doped TiO_2 (Hyd_0.1Fe). Although the other samples do not show a peak at ~400 eV indicative for the presence of nitrogen, the Ti $2p_{3/2}$ level found to be ~458 eV suggests some modification in the lattice due to nitrogen substitution. The oxygen 1*s* peaks at ~530.313 eV, for N-doped yellow TiO_2 (oxalhyd) and ~530.256 eV for Fe–N co-doped TiO_2 (Hyd_0.1Fe) are shown, respectively, in Fig. 3b and Fig. 3b″.

3.2.2. *Diffuse reflectance spectra (DRS)*

The DRS of the TiO_2 samples are shown, Fig. 4. The absorption is at <400 nm for white TiO_2, while the yellow colored TiO_2 indicates the absorption edge extending into the visible region, >400 nm.

A band gap, E_g1, of 3.26 eV was observed for the white TiO_2 that was calculated from Eq. (2) [32]

$$E_g = 1239.8/\lambda. \quad (2)$$

The wavelength λ of the absorption edge was taken from the peak position of the differential plots, which are also shown in the figure for ready reference. The yellow TiO_2, however, showed two peaks corresponding to band gaps: $E_g1 = 3.26$ and $E_g2 = 2.63$ eV, listed in Table 1. Two absorption bands

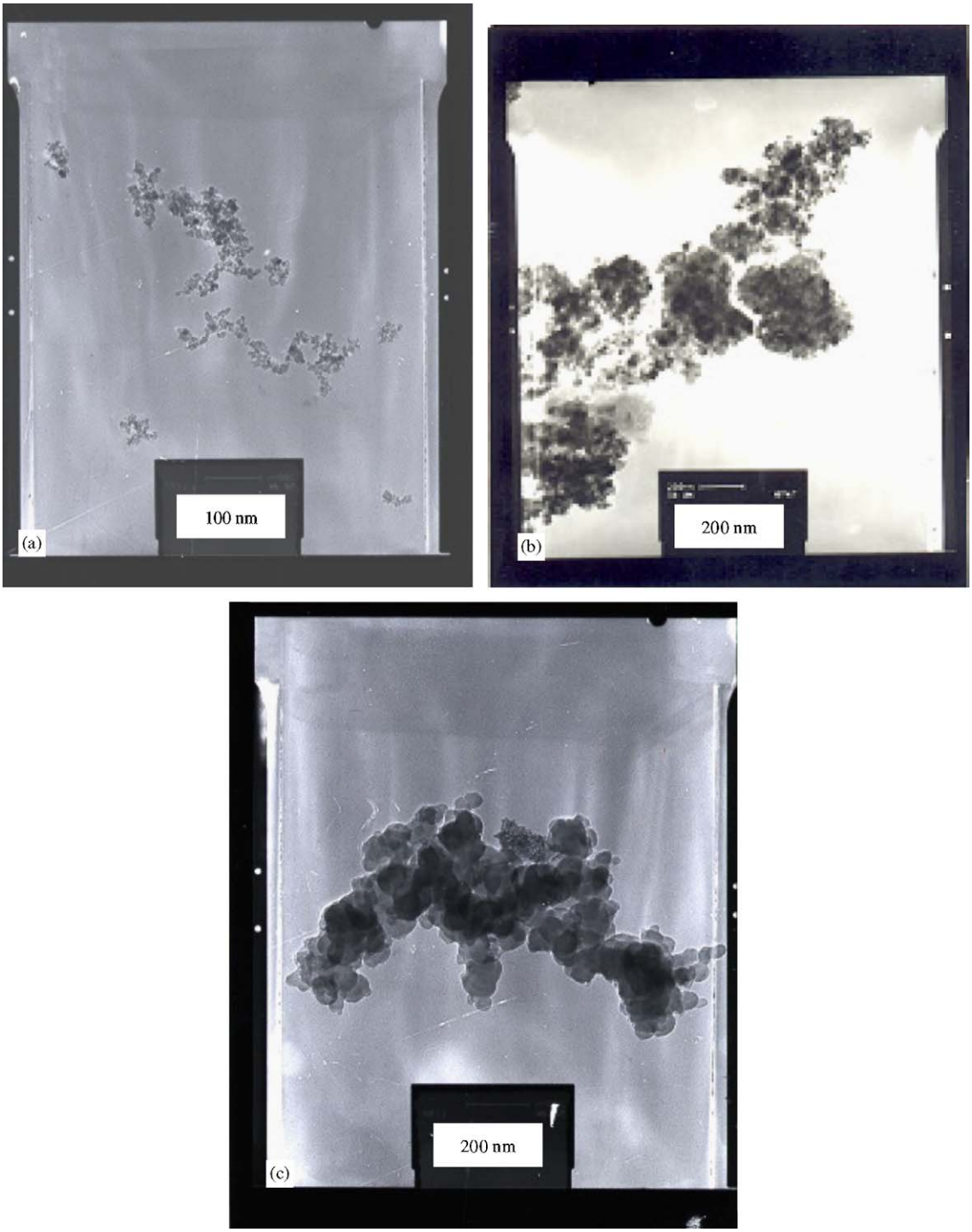

Fig. 2. TEM of (a) yellow TiO_2 (b) white TiO_2 and (c) Fe–N co-doped TiO_2, Hyd_0.01Fe.

at 400–408 nm (3.04–3.1 eV) and 530–550 nm (2.25–2.34 eV) are also observed [14] in the yellow powders obtained by planetary milling of the P-25 and hexamethylenetetramine (HMT). It is thought that the first and second edges are related to the band structure of the original titania and the newly formed N_{2p} band which is located above the O_{2p} valence band. The commercial white TiO_2, however, showed one band gap of 3.25 eV. All Fe-doped samples, Fig. 5, also show the absorption edge extending in the visible region and indicate two band gaps, Table 1.

However, the first band appears at 3.31, 3.38 and 3.05 eV, respectively, for 0.01, 0.05 and 0.1 Fe-doped samples without nitrogen. On the other hand, the Fe-doped samples containing nitrogen, Hyd_0.01Fe, Hyd_0.05Fe, Hyd_0.1Fe have the first band at ~2.8 eV which is much lower than 3.26 eV that observed for the yellow nitrogen-containing TiO_2. The

Table 1
Nitrogen content, BET surface area, band gap and % of photodegradation of 2-propanol and NO of all the TiO_2, N/Fe/Fe–N-doped TiO_2

Sample	N%	Surface area ($m^2 g^{-1}$)	Band gap, E_g1/E_g2 (eV)	Propanol degradation (%)	NO_x destruction (%)		
					>290	>410	>510 nm
WhiteTiO_2 Anatase, oxal	0.00	65.9	3.26/—	48.00	55.4	30.4	9.7
Yellow anatase,	0.95	107.6	3.25/2.63	19.00	42.3	25.8	12.3
oxalhyd Calcined in N_2/400 °C	0.30				54.2	37.5	18.8
White anatase							
TipOD	0.00	42.8	3.26/—	38.00	57.6	40.2	8.7
TipFD	0.00				69.5	40.2	7.6
Yellow anatase, TipODH Calcined in	0.13	48.4	3.25/2.63	20.00	49.5	25.8	12.4
N_2/400 °C	0.10				45.3	30.5	13.8
Degussa, P-25				58.00	43–53	Nil	Nil
0.01Fe-anatase/oxal	0.00		3.31/2.44	14.00	42.4	32.69.8	
0.05Fe-anatase/oxal	0.00		3.38/2.44	5.00	42.4	32.6	10.8
0.1Fe-anatase/oxal	0.00		3.05/2.44	4.00	31.9	11.0	6.8
Hyd_0.01Fe	0.425		2.8/2.41	2.00	42.8	30.8	24.2
Hyd_0.05Fe	0.576		2.79/2.41	10.00	39.6	25.3	13.0
Hyd_0.1Fe	0.796		2.80/2.36	0.00	19.4	8.6	7.5

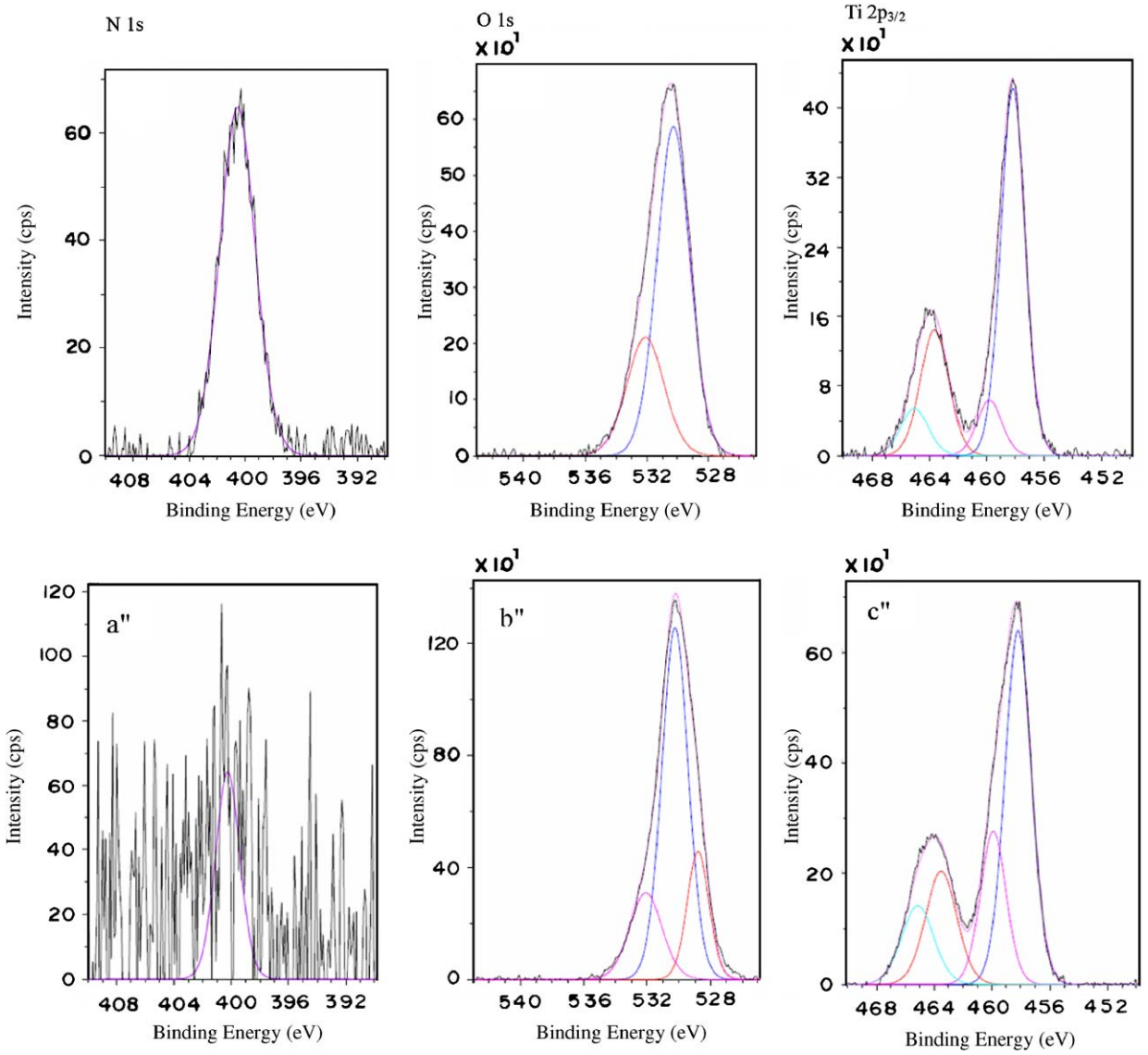

Fig. 3. XPS of N 1*s*, oxygen 1*s* and Ti $2p_{3/2}$ core levels of yellow $TiO_{2-x}N_x$, oxalhyd (a,b,c) and 0.1 Fe–N co-doped TiO_2, Hyd_0.1Fe (a″, b″, c″).

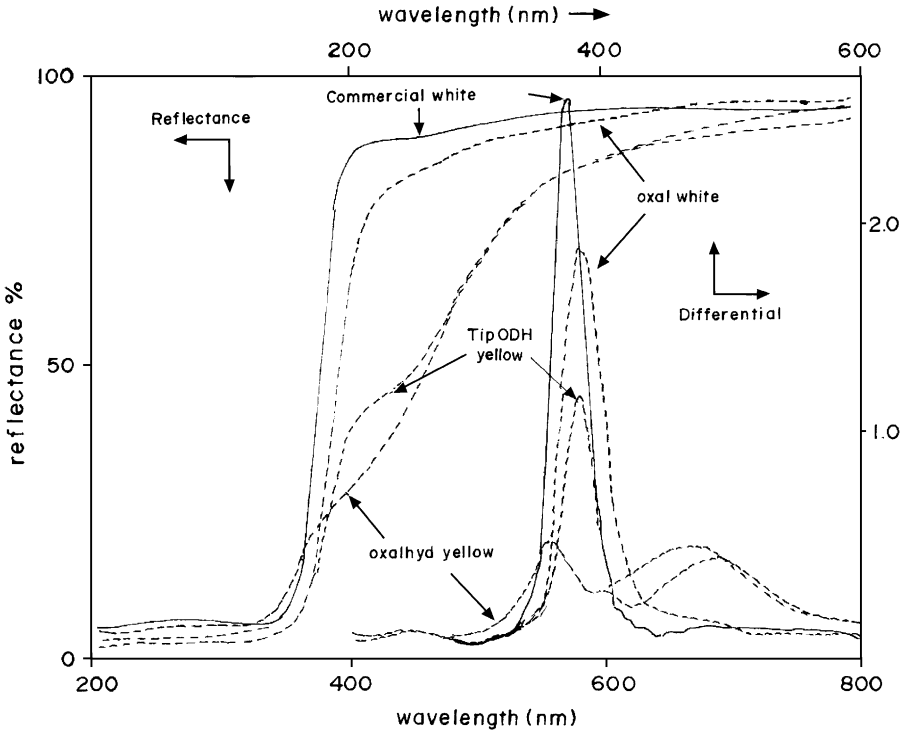

Fig. 4. DRS of TiO_2 and corresponding differential plots.

second gap, however, is at ~2.44 eV for all Fe-doped samples. These results suggest that iron doping modifies the first band gap of the white TiO_2 and introduces a second gap as in yellow N–TiO_2. But the second gap of N–TiO_2 is lowered by iron doping. The increase in the first band gap by Fe doping in TiO_2 from 3.26 to 3.38 eV and a decrease to 2.8 eV by co-doping of Fe and N suggest that there occur a lot of electronic structure changes due to doping. The study further suggests that a mid band gap is created. Anatase is a wide band gap (3.2 eV) insulator, and the changes in electronic structure must, therefore, reflect in their electrical characteristics. Hence the direct current electrical conductivity measurements were carried out on all samples to get some information on their semiconducting properties.

3.3. DC electrical conductivity, ESR

The temperature variation of direct current electrical conductivity of the samples (Fig. 6) shows a linear decrease in the conductivity with the increase in temperature, thereby, satisfying the Arrhenius equation, Eq. (3)

$$\sigma = Ae^{-E/kT} \tag{3}$$

where, σ is the conductivity; E the activation energy for producing free electrons or holes; T the absolute temperature, k the Boltzmann's constant; and A the constant. From the Arrhenius plot of $\log\sigma$ vs. $1/T$, activation energy of 1.8 eV was calculated from the linear range. These studies indicate that the oxides are semiconducting. It can be observed from Fig. 6 that the yellow colored $TiO_{2-x}N_x$ (TipODH) shows higher conductivity as compared to the white TiO_2 (oxal). The semiconducting white TiO_2 may have non-stoichiometric composition $TiO_{2-\delta}$. All Fe and Fe–N co-doped anatase with composition, $Ti_{1-y}Fe_yO_{2-x}N_x$, have higher resistance as compared to the yellow N-doped TiO_2.

An electronic semiconductivity is observed [33] in anatase and rutile due to free electrons as current carriers and an activation energy of 1.7 eV is found for rutile from an Arrhenius plot. From the variation in conductivity with the oxygen pressure, it is considered that there occurs an oxygen vacancy which contributes to electronic conductivity. TiO_2 is a reducible oxide and therefore the valence of the Ti can be changed from stable Ti^{4+} to the trivalent, Ti^{3+}, which has a $3d^1$ electronic configuration and can be identified [34] using electron paramagnetic resonance, EPR.

3.3.1. Electron spin resonance (ESR)

Sol–gel-derived TiO_2 showed one single first-derivative absorption line (line width of 0.6 mT) with $g = 1.998 \pm 0.004$ and the sample on hydrogen reduction indicated a pronounced peak. Based on these observations, the authors confirmed the presence of Ti^{3+} in TiO_2. The ESR spectra of all TiO_2 and Fe-doped TiO_2 samples, Fig. 7, show a band at $g = 1.994$–2.0025 with $\Delta H = 170$–210 G.

The measurements were carried out both at room temperature (RT) and liquid nitrogen temperature (LT). There seems to be broadening of the band for the nitrogen-doped sample. ESR performed on nano-colloid TiO_2 showed a resonance at g~2.0035 which is attributed to an oxygen hole center created near the surface that significantly increased with nitridation [35]. UV-irradiated TiO_2 show $\{>Ti^{IV}–OH\}$ radicals [36] with g_1 of 2.016 and

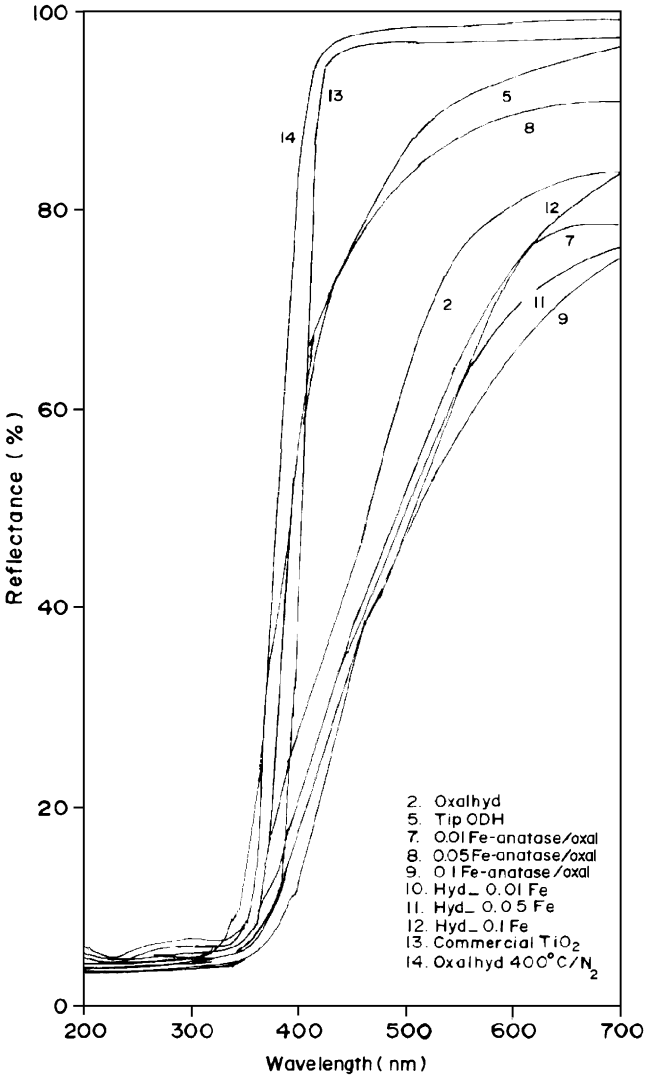

Fig. 5. DRS of TiO_2, N/ Fe–N-doped TiO_2.

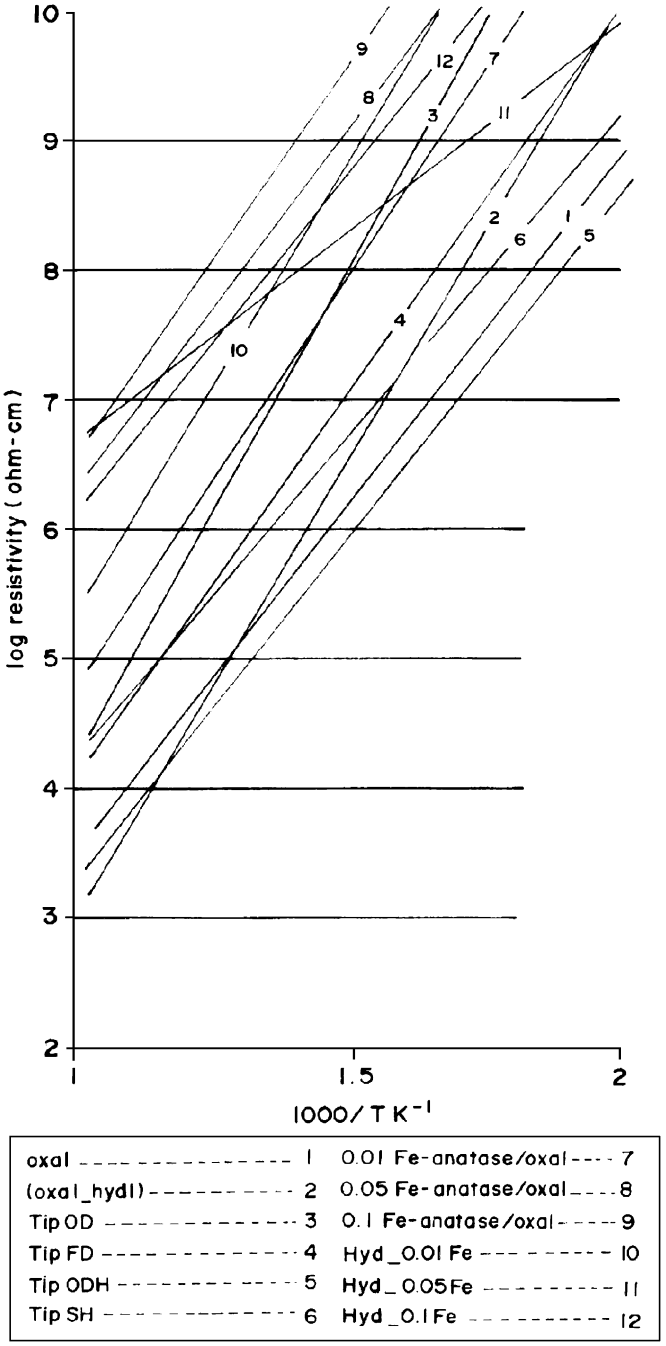

Fig. 6. Temperature variation of electrical resistivity of TiO_2 and Fe-doped TiO_2.

g_2 of 2.002 that arise from hole trapping, and in addition another peak with g value of 1.991, which is attributed to $\{>Ti^{III}–OH\}$ generated from trapping of excited electron. Fe-doped TiO_2 samples in the present investigations show a band with $g = 1.994–2.0025$, but they also have an additional peak at low field of $g = 4.19$ with $\Delta H = 125$ G. The EPR signal of soil sample for Fe^{3+} is observed at $g = 4.2$ [37]. $35TeO_2$ $(65-x)V_2O_5 \times Fe_2O_3$ (mol%) glasses show [38] ESR line at $g = 4.3$ due to Fe^{3+}. As the mol% of Fe_2O_3 increases the area under $g = 4.3$ increases and broadening of the hyperfine starts to take place. Fe-doped TiO_2 in the present studies, thus, indicate the Fe^{3+} in the sample.

3.3.2. Mechanism of conductivity

Decrease in conductivity and increase in activation energy E_a with the increase of Fe/Ti mole ratio [39] is considered to be due to the fact that Fe ions dissolve in TiO_2, which is an n-type semiconductor. These facts suggest that the valence control can be described by the following Kroeger–Vink notation,

$$Fe_2O_3 + 1/2O_2 \rightarrow 2Fe'Ti + 4O^*O + 2h.$$

Electrons as the carrier of the electrical conductance decreased because of the formation of the holes, so E_a increased. Thin film anatase with activation energy of 0.65 eV reduced to 0.51 eV in the presence of trace amount of Fe [40]. As Fe doping concentration increased, the n-type anatase transformed into rutile at ~0.32 at% Fe. The Fe doping is not a simple substitutional one and new oxygen vacancies are induced by the presence of iron

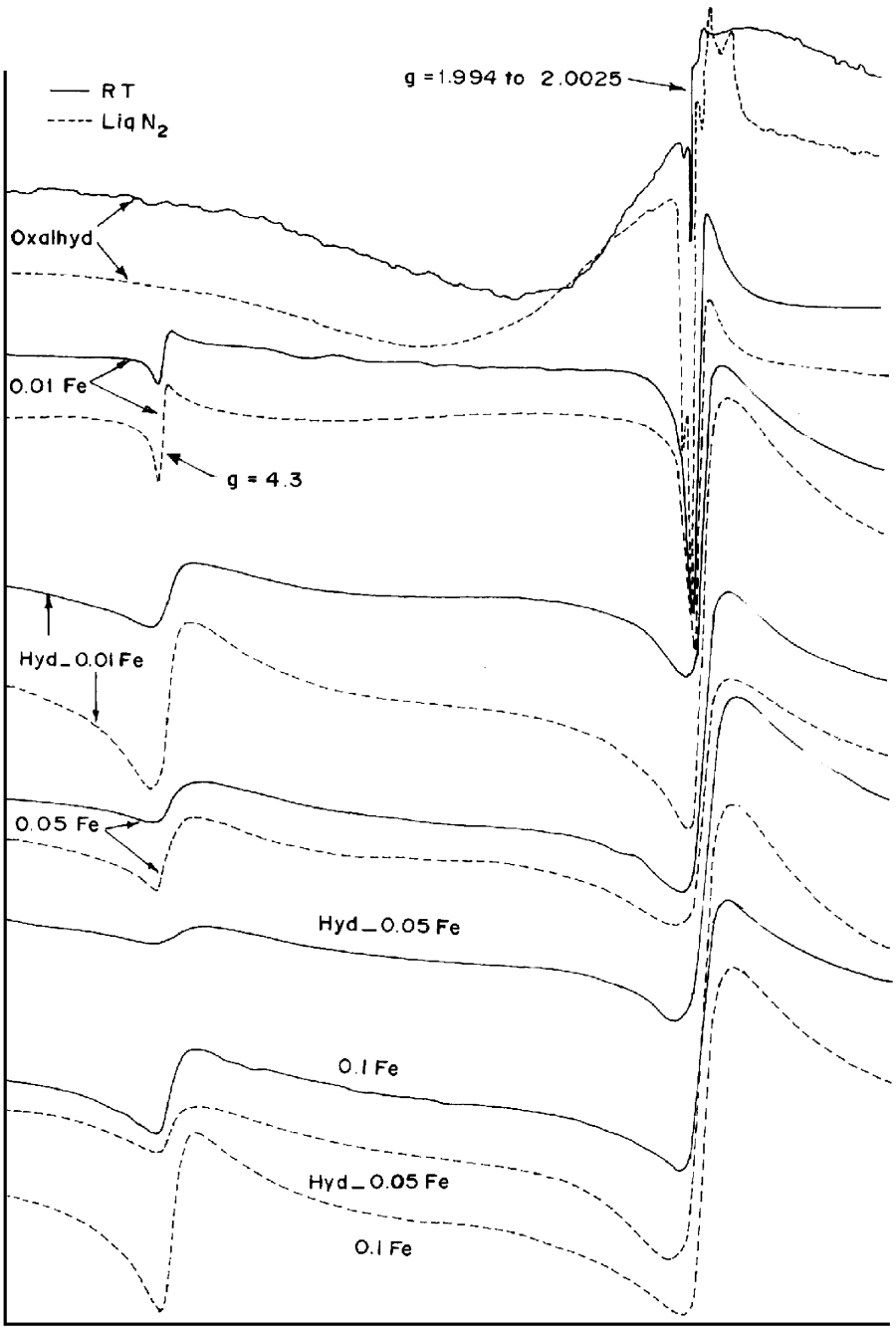

Fig. 7. ESR of TiO_2 and Fe-doped TiO_2.

atoms. Fe doped and Fe–N co-doped TiO_2 show the conductivity, Fig. 6, lower than that of the yellow TiO_2 (TipODH). The preliminary studies on the direct current electrical conductivity measurements in our present investigations, thus, do give indication of change in conductivity characteristics in the TiO_2 due to the presence of oxygen deficiency, nitrogen and Fe in the lattice.

There seems to be a correlation between the ESR studies and the electrical conductivity observations made here. The observation of activation energy ~1.8 eV from the Arrhenius plots and midgap band ~2.4 eV from DRS studies suggest possible presence of impurity levels in Fe–N-doped samples that cause the red shift in DRS. The red shift has been now considered to be due to N doping as well as by metal doping.

3.3.3. *Impurity levels in the wide band gap TiO_2*

There are controversies on locating the impurity levels in the band gap. Valentin et al. [41] in their studies on the photoactivity of N-doped anatase and rutile considered the N 2*p* localized states just above the top of the O 2*p* valence and in anatase these states cause a red shift of the

absorption edge towards visible region, while in rutile this effect is offset by the concomitant N-induced contraction of the O 2*p* band giving blue shift.

The doping of metal oxides with other elements is a well-recognized process in which the dopants produce electronic mid-gap states. Ultraviolet absorption in TiO_2 is due to its wide band gap of 3.2 eV and the band narrowing enables it to extend the absorption edge into the visible region as considered by Asahi et al. [21] for the N-doped $TiO_{2-x}N_x$ due to the mixing of N- 2*p* and O- 2*p* orbitals. Ihara et al. [42] on the other hand considered not only nitrogen in the lattice but also the oxygen vacancies and electronic levels slightly below the conduction band edge were responsible for the visible light response. The ESR signal observed at $g = 2.003$ supports the oxygen vacancy, as this signal is assigned to electron trapped at the oxygen defect site and it was observed that the signal gets strengthened when visible light illumination was applied. But, from their exhaustive photocurrent studies of non-doped and N-doped TiO_2, Nakamura et al. [27] gave a clear experimental evidence to the mechanism for visible light response by showing a N-induced mid gap level 0.75 eV above the valence band, which lies ~2.45 eV below the conduction band. The UV radiation produces the holes in the O 2*p* valence band which is 3.20 eV below the conduction band (the normal band gap of TiO_2) and visible light illumination produces the holes in the mid gap level that is 2.45 eV below the conduction band. Such mid gap bands are observed by us in our DRS studies of N-doped yellow TiO_2 and Fe doped (0.01/0.05/0.1 Fe-TiO_2) as discussed above (Table 1). However, the Fe–N co-doped samples (Hyd_0.01Fe, Hyd_0.05Fe, Hyd_0.1Fe) do show the mid gap band at ~2.40 eV, but there takes place a decrease in main band gap too from 3.2 band to 2.8 eV. Thus, there seems to be narrowing of the main band as well as introduction of the mid level gap in the Fe–N co-doped samples.

3.3.4. Photocurrent

The difference in the incident photon to current efficiency (IPCE) enhancement between UV and visible light illumination observed in the study of photocurrent measurements by Nakamura et al [27] to different reactivities of valence band and mid-gap level holes. Photocurrent measurements were thus considered to be important to get the insight in the mechanism of photocatalysis under UV and visible regions. The measurement of photocurrent during the reaction is of greater relevance than observing the products constitution in understanding the mechanism of photocatalysis involving the mid-gap and valence band holes. Such mid-gap states are indeed important in improving semiconducting properties of insulators, but in photocatalytic applications they are not desired, as these states trap the photogenerated holes and cause a decrease in the oxidation power of the catalyst. A reduced photocatalytic oxidation activity for 2-propanol and enhanced destruction activity for NO_x under visible irradiation as compared to the standard Degussa P-25 was observed. The results of such studies are discussed taking the clue of the presence of mid-gap level in the samples.

3.4. Photo-oxidation of 2-propanol and photodestruction of NO_x

The photodegradation of aqueous 2-propanol on all samples was carried out using a UV lamp ($\lambda > 245$ nm) at 295 K. The irradiation time was 2 h and in some cases the percentage degradation was measured at different intervals: 20, 40, 60 and 90 min. The gas phase NO_x destruction study was done at >290, >410 and >510 nm. The results of such studies are shown in Table 1.

About 20% 2-propanol degradation is observed for yellow N-doped TiO_2 (oxalhyd and Tiphyd), while the white TiO_2 (oxal) showed 48% conversion. The standard Degussa P-25 sample, however, showed higher conversion of 58%. A low percentage photo-oxidation of 2-propanol observed [18] on $TiO_{2-x}N_x$ with $0.005 \leqslant x < 0.02$ under visible light irradiation compared to UV irradiation is considered to be due to the formation of an N-induced narrow band slightly above the valence band. Similar low percentage degradation observations have been made by Nakamura et al. [27] from their photocurrent measurement studies on methanol, while from the analysis of the oxidized product of photocatalytic reactions of methylene blue [21], 2-propanol [18] and acetone [21,43] on N–TiO_2 it was observed that these reactions are possible under visible irradiation. Such discrepancies are due to no clear understanding of the mechanism of the reactions. Mrowetz et al. [44] fail to observe photocatalytic oxidation of $HCOO^-$ into CO_2^-, or of NH_3-OH^+ into NO_3^- under visible illumination by N-doped TiO_2 and authors of the opinion that any photo-catalytic oxidation of aqueous organic contaminants by such catalysts is conjectural one. However, Nakamura et al. [27] conclude their observations by considering N-induced (occupied) mid-gap level slightly above the valence band that is responsible for the visible light response. The white TiO_2 (oxal) is semiconducting non-stoichiometric and has one optical (DRS) band gap, $E_g1 = 3.26$ eV, while the yellow N-doped $TiO_{2-x}N_x$ shows two band gaps: $E_g1 = 3.25$ and $E_g2 = 2.63$ eV. And this presence of the mid-gap band may be the center for annihilating the charge carrier formed in the photoreaction causing the decrease in the degradation activity. The Fe-doped (0.01/0.05/0.1 Fe–TiO_2) and Fe–N co-doped (Hyd_0.01Fe; Hyd_0.05Fe; Hyd_0.1Fe-TiO_2) show less than 10% degradation, Table 1, thereby, indicating further decrease in the activity due to the presence of mid-gap band. The Fe–N co-doped TiO_2 may have this very low activity due to the mid-gap band at 2.42 eV, but they have their main band gap at a lower value of 2.8 eV, which may cause further annihilation of the charge carriers. On the other hand, all above samples have [45,46] significant NO destruction ability >290, >410 and >510 nm, Fig. 8, while the standard Degussa P-25 has no activity, in the visible region, >410 nm, Table 1.

The mid-gap bands seem to be advantageous in NO destruction activities; however, reasons as to why they are not so for the degradation of 2-propanol need to be

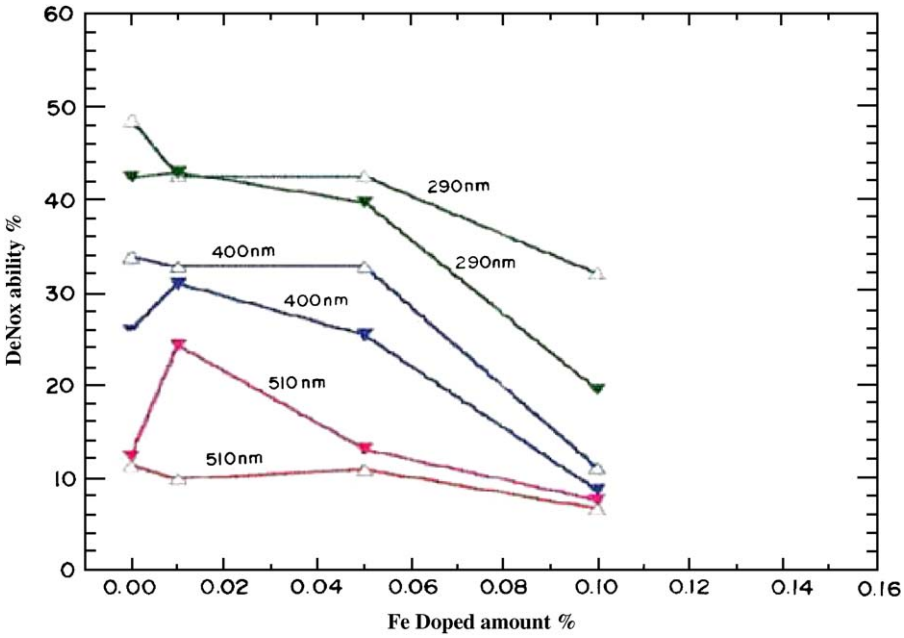

Fig. 8. NO_x destruction capacitiy of $TiO_{2-\delta}$ and Fe/Fe–N-doped TiO_2 in UV and visible regions; (open triangle = oxide from oxalate and shaded triangle = oxide from hydrazine method).

addressed. UV light in large band gap substances such as TiO_2 produces electron–hole pairs. The light-induced hole in the valence band combines with the water molecule to form hydroxyl group with powerful oxidation ability to degrade 2-propanol, while the electrons in the conduction band in the presence of oxygen and traces of moisture in the air (of the reaction mixture consisting of NO + Air and N_2 for balance in the present investigation) are trapped to generate active OOH^* radical. The nitrogen monoxide reacts with the reactive oxygen radical to produce HNO_2 or HNO_3. The mid-gap level may allow visible light to generate electrons and hence this is advantageous in NO destruction in our present studies. Hole produced in mid-gap level may not react with water molecule to produce hydroxyl oxidant. However, further elaborative studies need to be carried out to explore any possible correlation between the activation energy that was obtained from conductivity measurements and the mid-gap bands that were observed from the DRS studies in understanding the photocatalytic activities of anatase by choosing the other dopants such as Nb, Pt and Cr. The influence of surface area and crystal size of anatase on doping needs to be studied to determine their influence on catalytic activity.

4. Conclusions

i) Nitrogen-substituted yellow colored anatase, $TiO_{2-x}N_x$ and Fe–N co-doped TiO_2 have been readily synthesized by novel hydrazine method.
ii) White non-stoichiometric anatase form TiO_{2-x}, yellow $TiO_{2-x}N_x$, Fe-doped and Fe–N co-doped $Ti_{1-y}Fe_yO_{2-x}N_x$ are semiconducting and the ESR signals observed at $g\sim1.994$–2.0025 supports the oxygen vacancy, as this signal is assigned to electron trapped at the oxygen defect site and $g\sim4.3$ indicates the presence of Fe^{3+} in the lattice.
iii) UV absorption edge of anatase white TiO_2 extends to the visible region in yellow $TiO_{2-x}N_x$, Fe-doped and Fe–N co-doped TiO_2 and two band gaps are observed at $\sim$3.25/2.63 in N-TiO_2 and $\sim$3.31/2.44 and 2.8/2.44 eV, respectively, for Fe-doped and Fe–N co-doped TiO_2 suggesting possible mid-gap bands in the N, Fe and Fe–N doped anatase.
iv) The observation of activation energy $\sim$1.8 eV from the Arrhenius plots and mid-gap band $\sim$2.4 eV from DRS studies suggest possible presence of impurity levels in Fe–N-doped samples that cause the red shift in DRS.
v) All TiO_2 and Fe-doped TiO_2 show low 2-propanol photodegradation activity, but significant NO photo-destruction capability in both UV and visible region, while the standard Degussa P-25 has no activity in the visible region. The midgap bands may cause the discrepancy in their catalytic activities.

Acknowledgments

This work is partly supported by UGC (major project of KSR), DST (major project of Dr. B.R. Srinivasan and K.S.R.), DST-FIST and UGC-Special Assistance Programs of the Department of Chemistry, Goa University. K.S.R. is grateful to Dr. Gundu Rao, RSIC, IIT-Bombay for ESR spectra, Prof. M. Anpo and Dr. Neppolian of Osaka Prefecture University, Japan for ESCA and photodegradation of propanol investigations and useful discussions and Dr. Bindu Varughese of University of Maryland for XPS data.

References

[1] K.S. Rane, A.K. Nikumbh, A.J. Mukhedkar, J. Mater. Sci. 16 (1981) 2387.

[2] V. Moye, K.S. Rane, V.N. Kamat Dalal, J. Mater. Sci. Mater. Electron. 1 (1990) 212.

[3] V. Borker, K.S. Rane, V.N. Kamat Dalal, J. Mater. Sci. Mater. Electron. 4 (1993) 241.

[4] K.S. Rane, V.M.S. Verenkar, P.Y. Sawant, J. Mater. Sci. Mater. Electron. 10 (1999) 133.

[5] K.S. Rane, V.M.S. Verenkar, Bull. Mater. Sci. 24 (2001) 39.

[6] K.S. Rane, V.M.S. Verenkar, P.Y. Sawant, Bull. Mater. Sci. 24 (2001) 331.

[7] V.M.S. Verenkar, Beneficiation of Goan Ore Rejects to get pure iron oxide and utilization of the iron ore rejects to synthesize ferrites-high-tech magnetic materials, Ph.D. Thesis, Goa University, Goa, India, 1997.

[8] P. Y. Sawant, Physico-chemical methods to determine the trace elements in Goan Ore Rejects and beneficiate the ore to get pure iron oxides useful for high-tech ferrite manufacture, Ph.D. Thesis, Goa University, Goa, India, 1998.

[9] R. M. Pednekar, Synthesis and characterization of metal and mixed metal oxides of spinel and perovskite structure, Ph.D. Thesis, to Goa Univeristy, Goa, India, November 2005.

[10] R. Mhalsikar, K. S. Rane, A novel precursor technique to prepare yellow color TiO_2, in: Proceedings of the third National Symposium and Conference on Solid State Chemistry and Allied Areas, Indian Association of Solid State Chemists and Allied Scientists-ISCAS, IIT Delhi, India, p. 73 (P-30).

[11] K. S. Rane, Tailoring of electric, magnetic magnetic materials, in: Proceedings of the 19th Annual Symposium and Prof. Ram Chand Paul Second Symposium on Recent Trends in Chemistry, Punjab University, Chandigarh, India(Invited Lecture IL -4).

[12] R. Mhalsikar, R. Pednekar, K.S. Rane, Electrical characteristics of TiO_2 synthesized from different precursors, in: D. Bahadur, S. Vitta, O. Prakash (Eds.), Inorganic Materials: Recent Advances, Narosa Publishing House, New Delhi, India, Paper presented at the International Symposium in Inorganic Chemistry, IIT-Bombay, Mumbai, India, December 11–13, 2002, pp. 469–471.

[13] S. Sakthivel, H. Kish, Chemphyschem 4 (2003) 487.

[14] S. Yin, H. Yamaki, M. Komatsu, Q. Zhang, J. Wang, Q. Tang, F. Saito, T. Sato, J. Mater. Chem. 13 (2003) 2996.

[15] S. Yin, Q. Zhang, F. Saito, T. Sato, Chem. Lett. 32 (2003) 358.

[16] J.L. Gole, J.D. Stout, C. Burda, Y. Lou, X. Chen, J. Phys. Chem. B 108 (2004) 1230.

[17] H. Noda, K. Oikawa, T. Ogata, K. Matsuki, H. Kamata, Chem. Soc. Jpn. 8 (1986) 1084 ($TiCl_4 + (NH_2)_2 \cdot H_2O$ yellow colr due to oxygen vacancy).

[18] H. Irie, Y. Watanabe, K. Hashimoto, J. Phys. Chem. B. 107 (2003) 5483.

[19] M. Anpo, Catal. Surv. Jpn. 1 (1997) 169.

[20] M. Anpo, M. Takeuchi, J. Catal. 216 (2003) 505 (and references therein).

[21] R. Asahi, T. Morikawa, T. Ohwaki, K. Aoki, Y. Taga, Science 293 (2001) 269.

[22] I.A. Vogel, A Text Book of Quantitative Inorganic Analysis, Longman, UK, 1978.

[23] K. S. Rane, W. Weisweiler, H. Langbein, M. Crocoll, F. Kennfack, R. Pednekar, in: CGS Pillai, KL Ramkumar, PV Ravindran, V Venugopal, (Eds.), Proceedings of the 13th National symposium on Thermal Analysis-Thermans-2002, Indian Thermal Analysis Society, Mumbai, India, p. 145.

[24] ICDD Card # 02-0387.

[25] E.W. Schmidt, Hydrazine and its Derivatives, Wiley, New York, 1984.

[26] O. Diwald, T.L. Thopson, G. Goralski, S.D. Walck, J.T. Yates Jr., J. Phys. Chem. B 108 (2004) 52.

[27] R. Nakamura, T. Tanaka, Y. Nakato, J. Phys. Chem. B 108 (2004) 10617.

[28] S. Sakthivel, M. Janczarek, H. Kisch, J. Phys. Chem. B 108 (2004) 9384.

[29] C.D. Valentin, G. Pacchioni, A. Selloni, S. Livraghi, E. Giamello, J. Phys. Chem. B 109 (2005) 11414.

[30] X. Chen, C. Burda, J. Phys. Chem. B 108 (2004) 15446.

[31] M. Satish, B. Vishwanathan, R.P. Vishwanath, C.S. Gopinath, Chem. Mater. 17 (2005) 6349.

[32] B. Oregan, M. Gratzel, Nature 353 (1991) 737.

[33] M.D. Earle, Phys. Rev. 61 (1942) 56.

[34] E. Munoz, J.L. Boldu, E. Andrade, O. Navaro, X. Bokhimi, T. Lopez, R. Gomez, J. Am. Ceram. Soc. 84 (2001) 392.

[35] S.M. Prokes, J.L. Gole, X. Chen, C. Burda, W.E. Carlos, Adv. Funct. Mater. 15 (2005) 161.

[36] T.K. Kim, M.N. Lee, S.H. Lee, Y.C. Park, C.K. Jung, J.-H. Boo, Thin Solid Films 475 (2005) 171.

[37] B. Sutter, T. Wasowicz, T. Howard, L.R. Hossner, D.W. Ming, Soil Sci. Soc. Am. J. 66 (2002) 1359.

[38] R. Singh, J. Phys. D 17 (1984) L57–L60.

[39] N. Uekawa, Y. Kurashima, K. Kakegawa, Y. Sasaki, J. Mater. Res. 15 (2000) 967.

[40] A.R. Bally, E.N. Korobeinikova, P.E. Schmid, F. Levy, F. Bussy, J. Phys. D 31 (1998) 1149.

[41] C.D. Valentin, G. Pacchioni, A. Selloni, Phys. Rev. B 70 (2004) 085116.

[42] T. Ihara, M. Miyoshi, Y. Iriyama, O. Matsumoto, S. Sugihara, Appl. Catal. B 42 (2003) 403;
T. Ihara, M. Miyoshi, M. Ando, J. Mater. Sci. 36 (2001) 4201.

[43] Y. Sakatani, J. Nunoshige, H. Ando, K. Okusako, H. Koike, T. Takata, J.N. Kondo, M. Hara, K. Domen, Chem. Lett. 32 (2003) 1156.

[44] M. Mrowetz, W. Balcerski, A.J. Cloussi, M.R. Hoffmann, J. Phys. Chem. B 108 (2004) 12269.

[45] K. S. Rane, R. Mhalsikar, T. Sato, Shu. Yin, Kuk Cho, E. Dunbar, P. Biswas, Photocatalytic destruction of NO on N- and Fe–N co-doped anatase TiO_2, in: Proceedings of the fourth National Symposium and Conference of Solid State Chemistry and Allied Areas, Indian Association of Solid State Chemsts and Allied Scientists—ISCAS, Goa, 1–3 December 2005.

[46] K.S. Rane, Visible light sensitive TiO_2 photocatalyst, in: Proceedings of the Singapore International Chemical Conference-4 (SICC-4), Singapore, 8–10 December 2005, p. 194 (Inivted Talk- 81-IMSC-A0489).